The International Journal of Advanced Manufacturing Technology (2019) 102:305–314
https://doi.org/10.1007/s00170-018-3176-2

ORIGINAL ARTICLE

Prediction of surface roughness in milling process using vibration signal analysis and artificial neural network

T. Y. Wu [1] · K. W. Lei [1]

Received: 30 August 2018 / Accepted: 11 December 2018 / Published online: 3 January 2019

Abstract
The objective of this study is to investigate the feasibility of utilizing the signal features in vibration measurements during the milling process and the cutting parameters for predicting the surface roughness of S45C steel. The features of vibration signals are extracted by means of the envelope analysis, statistical computation, such as RMS (root-mean-square), kurtosis, skewness, and multi-scale entropy (MSE), as well as the frequency normalization. Through the correlation analysis, the features of higher priority are sifted out so that the prediction computation efforts can be reduced. The sifted vibration signal features are then collected as the input layer parameters of artificial neural network (ANN) for surface roughness prediction. The prediction results and accuracy through using different classes of input features are also discussed and compared. The experimental results show that the surface roughness is affected not only by the cutting parameters, but also by the vibration behavior during the milling process. Therefore, the cutting parameters combining the essential vibration features can be utilized to enhance the prediction accuracy of surface roughness during the milling process.

Keywords Milling · Surface roughness · Correlation analysis · Artificial neural network (ANN) · Envelope analysis · Multi-scale entropy (MSE) · Frequency normalization

1 Introduction

The prediction of surface roughness under milling/cutting process is essential for the tooling machine design and manufacturing process, and has attracted numerous researchers and engineers to dedicate the efforts to the related studies. Karayel [1] utilized the parameters of cutting speed, feed rate, and cutting depth for artificial neural network (ANN) modeling and then controlled the surface roughness of workpiece. Asiltürk and Çunkaş [2] employed the ANN and multiple regression method to predict the surface roughness of AISI1040 under different levels of cutting speed, feed rate, and cutting depth. They indicated that the more accurate prediction results can be obtained by the ANN model than by the multiple regression method.

Except for the cutting parameters combining the neural network models as well as the multiple regression methods, the signal measurements during the machining can be also utilized to predict the surface roughness of the workpieces. A linear regression model was applied for the surface roughness prediction of steel NAK80 by using the displacement sensors that was installed on the spindle [3]. Abouelatta and Mádl [4] proposed an approach for the surface roughness prediction of steel workpiece in turning operation. In their study, the multiple regression prediction model was established through the cutting parameters as well as fast Fourier transform (FFT)–based spectral features of the vibrating acceleration signals that were measured on the cutting tool. In addition, Abu-Mahfouz et al. [5] utilized the statistical features of vibration signals, such as mean, kurtosis, skewness, and standard deviation, to predict the surface roughness of workpiece in end milling operation. Their investigation indicated that the prediction accuracy can be enhanced by combining the principal component analysis (PCA) and the cutting parameters of cutting speed, feed rate, and cutting depth. Alternatively, a fuzzy net model was used to predict the surface roughness of alloy in turning operations [6]. The features of the fuzzy net were extracted from the vibration signals of the spindle,

✉ T. Y. Wu
tianyauwu@dragon.nchu.edu.tw

[1] Department of Mechanical Engineering, National Chung Hsing University, Taichung City, Taiwan

and the cutting parameters, including the feed rate and spindle rotating speed.

According to the previous literature of vibration signal analysis, the empirical mode decomposition (EMD) method is capable of separating the complicated signal into the intrinsic mode functions (IMFs) of different frequency scales such that the non-information-included signal components can be filtered out without the occurrence of phase shift and waveform distortion [7]. On the hand, the previous study [8] indicated that the entropy of vibration signals represents the complexity or regularity of the data series that is intuitively related to the system dynamical behavior. Therefore, the multi-scale entropy (MSE) of the measured signals can reveal the tiny variation of machine dynamics in terms of the entropy values of different scales [9]. Alternatively, the measurements of cutting force were utilized to predict the surface roughness during the ball-end milling process through the wavelet transform approach [10]. An ANN-based monitoring system was developed to predict the dynamic surface roughness by using the various cutting parameters, material types, coolant fluid, and machine vibrations as the inputs [11].

Based on the previous studies in the previous literature related to the surface roughness prediction of milling process, it is found that the surface roughness of workpiece is attributed not only to the combinations of cutting parameters, but also to the influence from machine vibrations in the milling process. Since the studies of cutting parameters have been conducted to examine the correlation of surface roughness extensively, the vibration measurement analysis and feature extraction techniques become the major challenge of enhancing the accuracy of surface roughness prediction. In this research, the features that are related to the surface roughness of workpiece in milling process were extracted from the vibration signals of spindle and vise as well as their relative vibrating motions. To advance the state-of-art of the surface roughness prediction, the EMD method was utilized to remove the signal components that contain noises and useless information. The features that include the kurtosis, skewness, and MSE in time domain as well as the spectral levels in frequency domain were determined and extracted. On the other hand, in order to remove the factor of feature variation in the cases of different spindle rotating speed, the frequency normalization technique [12] was utilized to extract the rotation speed–related features in the order spectra. Furthermore, the workpiece in milling process normally reveals the periodic surface profiles, it can be inferred that the vibration signals may present the amplitude modulation phenomenon that is not broadly investigated for the surface roughness prediction in the previous studies. Therefore, the features of the corresponding envelope signals were also extracted in this research. The correlation between the extracted features and the surface roughness was then analyzed by using the Pearson correlation coefficient.

The proposed prediction approach was verified experimentally by the milling process of S45C steel. The surface roughness of the workpiece was predicted through the sifted features and using the trained ANN. The prediction of using different classes of input features are discussed and compared in this study. The results demonstrate that the proposed approach is effective to accurately predict the surface roughness of milling process. For the purpose of further usage and reference, all the vibration measurements as well as the corresponding surface roughness average (R_a) values and the cutting parameters that were utilized in this research article are available at the website (http://web.nchu.edu.tw/~tianyauwu/data/ra_s45c/ra_s45c.htm).

2 Vibration signal feature extraction and feature classification

2.1 Envelope analysis

In the cutting process, the blades of tool impact the workpiece cyclically and thus induce a periodic vibration behavior. It is normally observed that the vibration measurements contain the amplitude modulating phenomenon. Therefore, the envelope analysis can be employed to demodulate the vibration signals and to extract the surface roughness–related features of signal envelope. The envelope of the vibration signal can be determined in terms of the complex analytical signal $z(t)$ which is obtained through the Hilbert transform [13],

$$z(t) = x(t) + jH[x(t)] = A(t)e^{j\varnothing(t)}, \quad (1)$$

where $x(t)$ represents the vibration signal, $H[.]$ represents the Hilbert transform, and $A(t)$ is the envelope of the vibration signal. For the vibration measurement with amplitude modulation, the envelope analysis is one of the important means to extract the signal features in the time domain.

2.2 Empirical mode decomposition

The vibration measurements may contain useless noise and unrelated signal components at different frequencies inevitably. In order to extract the surface roughness–related features in certain frequency range, the signal decomposition or filtering process is needed to separate the complicated measurement into the signal components of specific frequency bands. The empirical mode decomposition (EMD) method is an adaptive signal separation method and is capable of decomposing the complicated signal into a number of IMFs of different frequency range, that is [13].

$$x(t) = \sum_{i=1}^{n} c_i(t) + r_n(t), \quad (2)$$

where $x(t)$ represents the vibration signal, $c_i(t)$ is the i-th IMF, and $r_n(t)$ represents the signal residue or trend. Each IMF represents a mono-oscillating component within a narrow frequency band, and thus satisfies the following conditions [13]: (i) The number of extrema and the number of zero-crossings must be either equal or differ at most by one in the whole data set; (ii) At any point, the mean value of the envelope defined by the local maxima and the envelope defined by the local minima is zeros.

The EMD method is equivalent to a band-pass filtering process and can be used to reconstruct the information-contained signal within the specific frequency range without the drawbacks that the normal filtering process may encounter. It is beneficial to extract the surface roughness–related features from the signal within the certain frequencies.

2.3 Multi-scale entropy

The concept of entropy in the information theory is usually applied to estimate the complexity of the observation data which is capable of characterizing the system dynamical behaviors. Shannon proposed the method to compute the entropy of the series data, and then the method has been utilized to measure the complexity or disorderliness of signals [14]. For a given discrete series $\mathbf{S} = \{x_1, x_2, ..., x_N\}$, it has N outcomes in which there exist n classes ($\{s_1, s_2, ..., s_n\}$). The entropy of the series $\mathbf{S}$ is computed as:

$$\mathrm{En}(\mathbf{S}) = -\sum_{i=1}^{n} p(s_i)\log(p(s_i)), s_i \in \mathbf{S}, 1 \le i \le n. \tag{3}$$

where $p(s_i)$ represents the probability density function of the series $\mathbf{S}$, and log represents the logarithmic function. The algorithm of determining the sample entropy (SE) of a series was developed subsequently by Richman and Moorman [15]. Let $\mathbf{S}$ be the same time series of data length of N, and m sequential points of the time series be a pattern. Therefore, the pattern space $\mathbf{X}$ is defined as [15]:

$$\mathbf{X} = \begin{bmatrix} x_1 & x_2 & \cdots & x_m \\ x_2 & x_3 & \cdots & x_{m+1} \\ \vdots & \vdots & \ddots & \vdots \\ x_{N-m+1} & x_{N-m+2} & \cdots & x_N \end{bmatrix}. \tag{4}$$

The mean self-similarity quantity is formulated as:

$$\varphi_m(r) = \frac{1}{(N-m)(N-m+1)} \sum_{i=1}^{N-m} \sum_{j=1}^{N-m+1} G(d_{ij}, r), \tag{5}$$

where $G(\cdot)$ represents the Heaviside function, r is the tolerance, and d_{ij} represents the distance between the i-th and j-th patterns, formulated as $d_{ij} = \|\mathbf{X}_i - \mathbf{X}_j\|$. It can be observed that the self-similarity quantity estimates the repetition degree of sequential pattern of length m. By calculating the self-similarity for the pattern space of the length of $m+1$, the sample entropy of the series is thus determined as:

$$\mathrm{SEn}(m, r) = -\log \frac{\varphi_{m+1}(r)}{\varphi_m(r)}. \tag{6}$$

Costa et al. [16, 17] proposed the concept of multi-scale entropy (MSE) to represent the regularity of the data series in different scales through the coarse-grain process. Their analysis results indicated that the utilization of MSE is capable of classifying the physiological signals of human beings among the healthy and pathological people. The coarse-grain process is mainly to transform the original data series into different scales. The given data series, $\mathbf{S} = \{x_1, x_2, ..., x_N\}$, is first segmented into several data sets of length τ. By taking the mean values of the segmented data according to the following formula, the new series sets $\mathbf{y}^{(\tau)} = \{y_j^{(\tau)}\}$ are then obtained:

$$y_j^{(\tau)} = \frac{1}{\tau} \sum_{i=(j-1)\tau+1}^{j\tau} x_i, 1 \le j \le \frac{N}{\tau}, \tag{7}$$

where τ is called the scale factor. As observing the formula of coarse grain, it is equivalent to the process of sliding window of length τ and taking the average of the data series within the window in the way of non-overlap. In other words, the coarse-grain process includes the steps of utilizing the moving average filter to remove the high-frequency components and having down-sampled signal. The MSE is then obtained by calculating the sample entropy SEn of $\mathbf{y}^{(\tau)}$ with different scale τ, that is,

$$\mathrm{MSE}(\mathbf{S}, \tau, m, r) = \mathrm{SEn}\left(\mathbf{y}^{(\tau)}, m, r\right). \tag{8}$$

It is noted that the tolerance r is set to be fixed while computing the SEn of different scales τ. Therefore, the MSE analysis is not affected by the original signal amplitude.

2.4 Pearson correlation analysis

In statistics, the Pearson correlation analysis is employed to measure the linear correlation between two data sets of variable series. The Pearson correlation coefficient $\rho_{\mathbf{AB}}$ between the data set $\mathbf{A} = \{a_1, a_2, \ldots, a_n\}$ and data set $\mathbf{B} = \{b_1, b_2, \ldots, b_n\}$ can be expressed as

$$\rho_{AB} = \frac{\sum_{i=1}^{n} (a_i - \bar{a})(b_i - \bar{b})}{\sqrt{\sum_{i=1}^{n} (a_i - \bar{a})^2} \sqrt{\sum_{i=1}^{n} (b_i - \bar{b})^2}}, \tag{9}$$

where $\bar{a}$ and $\bar{b}$ represent the mean values of data sets $\mathbf{A}$ and $\mathbf{B}$. The range of the correlation coefficient value is between −1 and 1. The two data sets have a total positive linear correlation if the correlation coefficient value is 1, representing the two data sets have a completely coincidental trend. While the

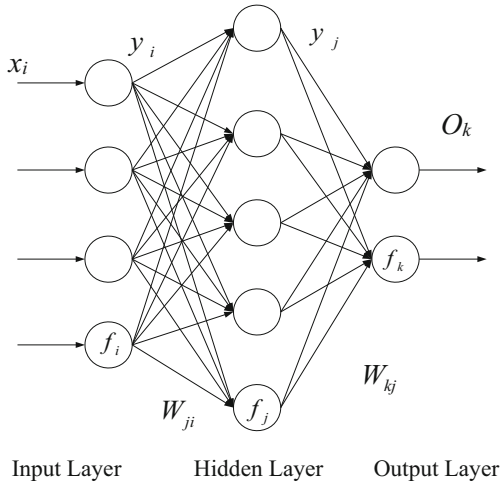

Fig. 1 Typical BPNN architecture

correlation coefficient value is − 1, the two data sets have a total negative linear correlation that represents the two data sets have a totally opposite trend. The correlation coefficient value of zeros means that the two data sets have no linear correlation.

2.5 Artificial neural network

The ANN is to imitate the learning mechanism in the biological neural networks of the brain. Since the ANNs are capable of processing the information flows in linear/nonlinear systems, they have been utilized in versatile applications, such as data classification, pattern recognition, and decision control. The back-propagation neural network (BPNN) [18] is one of the well-known ANN architectures and has been broadly applied to solve the problems in different fields. Figure 1 shows the typical BPNN architecture that consists of one input layer of the source nodes, one or more hidden layers of the computation nodes, and one output layer. According to the numbers of input and output variables in the system, the numbers of nodes in the input and output layers can be decided in the BPNN architecture. The numbers of hidden layers and nodes are usually decided depending on the computational efficiency and accuracy.

On the feed-forward stage, the input variables x_i are transmitted from the input nodes to the hidden layers. The input of the j-th node in the hidden layer net_j is formulated as

$$\mathrm{net}_j = \sum_i w_{ij} x_i + b_j \tag{10}$$

where w_{ij} and b_j represent the weight and bias from the i-th node of the input layer to the j-th node of the hidden layer, respectively. The output of the j-th node in the hidden layer is then calculated as

$$y_j = f\left(\mathrm{net}_j\right) \tag{11}$$

where $f(\bullet)$ represents the activation function that is often chosen as the sigmoid function,

$$f(t) = \frac{1}{1 + e^{-\alpha t}} \tag{12}$$

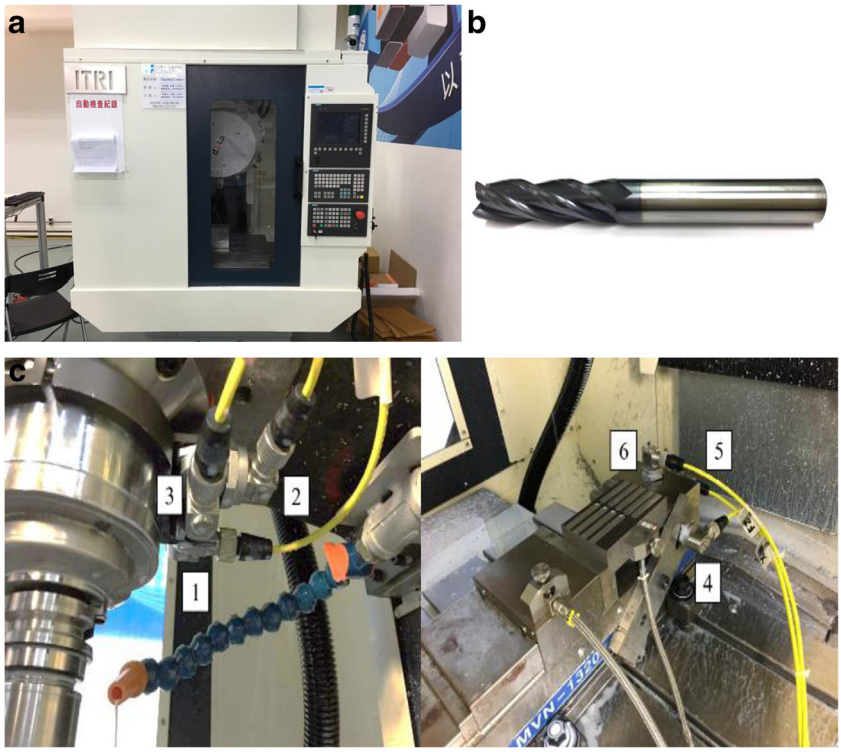

Fig. 2 **a** Picture of milling machine in this experiment. **b** Picture of tungsten carbide milling cutter in this experiment. **c** Picture of accelerometer installation on spindle (1–3) and vise (4–6)

Table 1 Specification of tungsten carbide milling cutter

Diameter of cutter blade	10 mm
Length of blade	30 mm
Total length of cutter	75 mm
Diameter of cutter Hilter	10 mm
Number of blade	4
Helix angle	35°

The output of the k-th node in the output layer is therefore formulated as

$$O_k = f(\text{net}_k) = f\left(\sum_j w_{jk} y_j + b_k\right) \quad (13)$$

The error function E is defined as the square of the difference between the actual output and the desired output,

$$E = \sum_i (d_i - O_i)^2 \quad (14)$$

where d_i is the i-th desired output. In the training process of the BPNN, if the error function E is large, the algorithm is executed at the back-propagation stage. During the back-propagation algorithm, the output is fed back to the hidden layers to adjust the weight values, such that the error function E is minimized. According to the principle of gradient descent, the weight value at the $n+1$ step can be derived as [18]

$$w_{jk}(n+1) = w_{jk}(n) + \gamma f'(\text{net}_k)[d_k(n) - O_k(n)] y_j(n) \quad (15)$$

where γ is the learning rate and $f'(\bullet)$ represents the first derivative of $f(\bullet)$. The weight values are updated repetitively until the error function E converges to an acceptable small value.

3 Experimental verification

3.1 Experimental setup

In order to verify the proposed approach and evaluate the accuracy of predicting the workpiece surface roughness, the tungsten carbide milling cutter was utilized to cut the steel S45C in the experiment. Figure 2a, b shows the pictures of the tooling machine and the cutter used in this experiment.

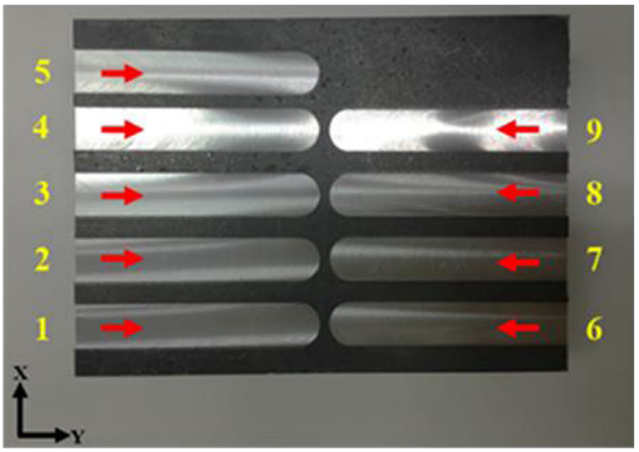

Fig. 3 Milling sequence and direction

The specification of the cutter is shown in Table 1. As shown in Fig. 2c, the accelerometers (Wilcoxon Research 785A) were stuck on the spindle and the vise to measure the vibration acceleration during the milling process. The main objective of this research was to utilize the signal processing techniques for vibration feature extraction and then demonstrate that the extracted features are eligible to enhance the accuracy of surface roughness prediction. Therefore, a simplified experiment setup was utilized, including cuboid steel block with straight-line cutting traces and three different clamping torque setting values of vise. The cutting parameters, including eight various values of spindle speed and nine various values of feed rate, can result in varying levels of the feed per tooth and thereafter the surface roughness variation of workpiece. Table 2 shows the different combinations of cutting parameters as well as the estimated removed volume accumulation (RVA) of the same cutter. The measured vibration signals were recorded by the data acquisition device (DAQ NI 9234) with the sampling rate of 10 KHz. The milling sequence and direction on the workpiece are shown in Fig. 3. It is intuitive that the cutter wear is one of the factors affecting the surface roughness during the milling process. In this research, the estimated RVA was utilized to represent the simplified cutter wear feature due to the limitation of instrumentation and quantification for tool wear inspection, such as the worn edge estimation through the online microscope. Each new cutter was only used in the milling

Table 2 Cutting parameters and estimated removed volume accumulation

Cutting parameter	Setup value
Spindle speed (rpm)	900, 1000, 1800, 1900, 2000, 2100, 2700, 3000
Feed rate (mm/min)	228, 240, 252, 320, 400, 420, 532, 560, 588
Feed per tooth (mm/tooth)	0.02–0.09 (total 10 levels)
Cutting depth (mm)	0.5, 0.6, 0.7, 0.8, 0.9, 1
Clamping torque of vise (N-m)	18, 30, 75
Removed volume accumulation (RVA) per cutter (mm^3)	Estimated value: 0–74.8

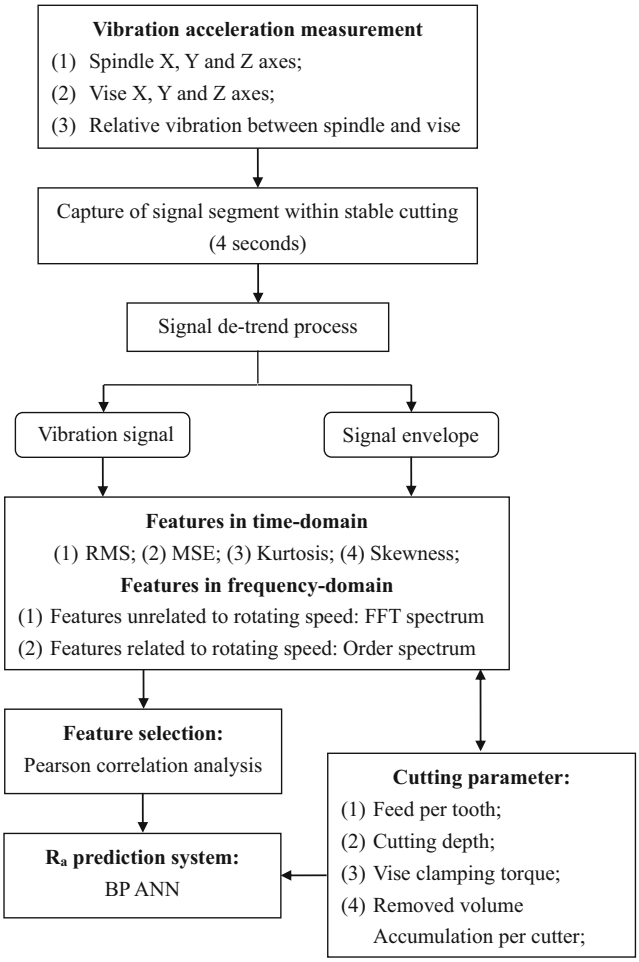

Fig. 4 Procedure of signal analysis and feature extraction

process of one block of workpiece (a total of nine cutting traces) in this experiment, and thus the estimated RVA was used to simply represent the factor of cutter wear. Once the milling process was finished for one block of workpiece according to the different setup combinations of cutting parameters, the surface roughness of workpiece was measured in terms of roughness average (R_a) by the instrument (Mitutoyo SV-C3200S4) which is capable of measuring the surface profile of workpiece within the range of 100 mm in *X*-axis and 8/80/800 μm in *Y*-axis with the corresponding resolution of 0.0001/0.001/0.01 μm. All the vibration measurements and the corresponding combinations of cutting parameters as well as the R_a values that were utilized in this research article are available at the website (http://web.nchu.edu.tw/~tianyauwu/data/ra_s45c/ra_s45c.htm). The same techniques and processes can be employed for the practical applications in manufacturing engineering.

Table 3 Pearson correlation coefficients between R_a and RMS

Signal category		*X*-axis	*Y*-axis	*Z*-axis
Spindle	Envelope	0.43	0.52	0.58
	Vibration	0.43	0.48	0.58
Vise	Envelope	0.13	0.12	0.22
	Vibration	0.10	0.12	0.16
Relative vibration between spindle and vise	Envelope	0.08	0.09	0.25
	Vibration	0.01	0.08	0.23

3.2 Vibration signal feature extraction

The steps of the vibration signal processing and analysis are divided into two parts. One part contains the signal feature extraction process in time domain, and the other part includes the FFT based spectrum analysis and feature extraction in frequency domain. The flowchart of vibration signal processing and analysis is shown in Fig. 4. The signals that were used for feature extraction consist of the vibration measurements in *X*, *Y*, and *Z* directions of the spindle, the vibration measurements in *X*, *Y*, and *Z* directions of the vise, and the relative vibration signals between the spindle and the vise in the three directions.

The first step of pre-processing the vibration signals was to capture the signal segment of 4 s within the stable cutting

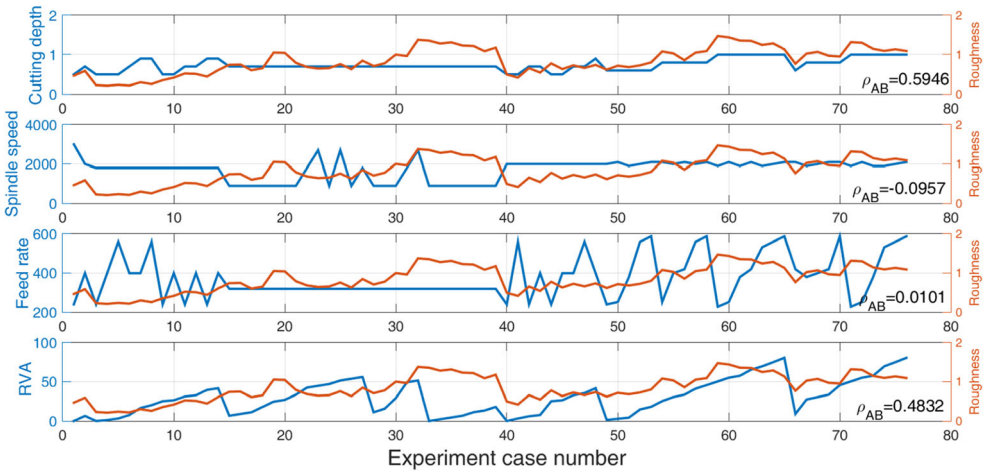

Fig. 5 Coherence between the R_a and cutting depth, spindle speed, feed rate, and RVA

Table 4 Pearson correlation coefficients between R_a and kurtosis

Signal category		*X*-axis	*Y*-axis	*Z*-axis
Spindle	Envelope	0.02	− 0.23	0.06
	Vibration	− 0.26	− 0.01	− 0.27
Vise	Envelope	0.03	0.03	0.13
	Vibration	0.05	− 0.08	− 0.01
Relative vibration between spindle and vise	Envelope	0.05	0.09	0.08
	Vibration	0.17	0.14	0.15

Table 5 Pearson correlation coefficients between R_a and skewness

Signal category		*X*-axis	*Y*-axis	*Z*-axis
Spindle	Envelope	− 0.20	− 0.04	− 0.13
	Vibration	− 0.08	− 0.17	− 0.13
Vise	Envelope	− 0.01	− 0.21	0.11
	Vibration	− 0.28	− 0.21	− 0.14
Relative vibration between spindle and vise	Envelope	0.09	0.17	0.19
	Vibration	0.17	0.07	0.11

process. The signal segments were then separated through the EMD method for the de-trend and filtering processes at the second step. Sequentially, the feature extraction was employed for the signal itself and its corresponding envelope.

In the time-domain feature extraction, the MSE, root-mean-square (RMS), kurtosis, and skewness of the vibration signals and their envelope were calculated as the features.

In the part of frequency-domain feature extraction, the frequency-domain features consisted of the rotation speed–related features as well as the rotation speed–unrelated features. The spectral distributions of the vibration signals and their envelope were computed in frequency domain through the FFT-based spectrum analysis. The spectral magnitude within 5000 Hz was extracted as the rotating speed–unrelated features, which consisted of the characteristics of the structural natural vibration, noises, and disturbances. In additional, since some of the frequency-domain features are variating with the rotating speed of the spindle, the FFT-based spectra were normalized by the rotating frequency to obtain the order distributions. Therefore, the rotation speed–related features were extracted from the order distributions.

3.3 Correlation analysis of feature

Figure 5 shows the coherence between the R_a values of workpiece and different cutting parameters to first demonstrate the R_a variation with respect to the cutting depth, spindle speed, feed rate, and RVA. It can be observed that the coherence between the R_a values of workpiece and different cutting parameters is not apparent since the highest correlation coefficient of 0.59 was computed among the different cutting parameters. It is inferred that the surface roughness cannot be predicted accurately only by utilizing the cutting parameters; therefore, the features of vibration signals can be used to enhance the prediction accuracy of workpiece surface roughness.

Once the R_a values of the workpiece surfaces were measured and all the vibration signal features were extracted in the time domain as well as the frequency domain, the correlation analysis was applied for selecting the specific features of high priority. Tables 3, 4, and 5 show the Pearson correlation coefficients between the R_a values and the RMS, kurtosis, and skewness features of vibration signals and their envelope signals on the three axes. As shown in these tables, it can be inferred that the correlation between RMS features and R_a values are much higher than those of kurtosis and skewness. Additionally, it is also noted in Table 3 that the correlation coefficients of *Z*-axis are higher than those of *X* and *Y* axes. It is quite reasonable since the R_a values represent the factor of surface profile on *Z* direction. Among them, on the other hand, the correlation coefficients of envelope signals are higher than those of vibration signals.

Similarly, the correlation coefficients between R_a values and MSE features within the first 20 scales were calculated to evaluate the correlation between the surface roughness of workpiece and the vibration signal complexity in different scales. The results of higher absolute values of Pearson

Table 6 Scales of MSE features with high correlation between R_a and MSE (Pearson correlation coefficient ≥ 0.4 or ≤ −0.4)

Spindle *Y*-axis	Envelope	Scale	1	2				
		Correlation coefficient	− 0.44	− 0.43				
Spindle *Z*-axis	Envelope	Scale	1	2				
		Correlation coefficient	− 0.46	− 0.44				
Relative vibration *Y*-axis	Envelope	Scale	3	4	5	6		
		Correlation coefficient	− 0.44	− 0.44	− 0.41	− 0.41		
Relative vibration *Z*-axis	Envelope	Scale	3	4	5	6	7	8
		Correlation coefficient	− 0.43	− 0.42	− 0.42	− 0.42	− 0.41	− 0.40

Table 7 Order features with high correlation between R_a and magnitude (Pearson correlation coefficient ≥ 0.5 or ≤ −0.5)

Spindle *X*-axis	Vibration signal	Order	17	34	38	
		Correlation coefficient	0.51	0.51	0.50	
Spindle *Y*-axis	Vibration signal	Order	13	17	26	34
		Correlation coefficient	0.51	0.52	0.51	0.52
Spindle *Z*-axis	Vibration signal	Order	13	17	34	38
		Correlation coefficient	0.50	0.53	0.52	0.51
	Envelope	Order	34			
		Correlation coefficient	0.51			
Relative vibration *X*-axis	Vibration signal	Order	17	34	38	
		Correlation coefficient	0.50	0.50	0.50	
Relative vibration *Y*-axis	Vibration signal	Order	13	17	34	38
		Correlation coefficient	0.52	0.53	0.51	0.50
	Envelope	Order	34			
		Correlation coefficient	0.50			
Relative vibration *Z*-axis	Vibration signal	Order	13	17	34	38
		Correlation coefficient	0.51	0.54	0.51	0.52
	Envelope	Order	34	38		
		Correlation coefficient	0.53	0.50		

correlation coefficients are shown in Table 6. It is observed that the MSE values in certain scales have obvious negative correlation with the surface roughness of workpiece. Overall speaking, the envelope signals have more high-correlated features with the R_a values than the vibration signals in the time domain.

The correlation analysis was also employed for all the extracted frequency-domain features. Tables 7 and 8 show the order and frequency features in which the Pearson correlation coefficients between the R_a values and the frequency-domain features are higher than 0.5. As noted in the two tables, the vibration signals have higher correlation with the surface roughness of workpiece than those of their envelope. It is also observed similarly that the correlation coefficients on *Z*-axis are higher than those on *X* and *Y* axes. Overall speaking, the vibration signals have more high-correlated features with the R_a values than their corresponding envelope signals in frequency domain.

3.4 Prediction result of artificial neural network

In order to demonstrate the R_a prediction performance of the proposed approach, the ANN was employed to train the prediction model. In this research, different classes of features were selected to evaluate the prediction accuracy for comparison purpose. The features of the first class in the input layer of ANN include the cutting parameters, which are feed per tooth, cutting depth, clamping torque of vise, and the RVA per cutter. The features extracted from the vibration signals were selected in the second class if their correlation coefficients to R_a values have absolute values higher than 0.4. The third class consists of the features of the cutting parameters as well as the selected features of the second class. In the R_a prediction process of ANN model, half the features were randomly selected for model training, and the remaining half features were utilized to verify the R_a prediction results. The

Table 8 Frequency features with high correlation between R_a and magnitude (Pearson correlation coefficient ≥ 0.5 or ≤ −0.5)

Spindle *X*-axis	Vibration signal	Frequency (Hz)	580.8				
		Correlation coefficient	0.50				
Spindle *Y*-axis	Vibration signal	Frequency (Hz)	580.8				
		Correlation coefficient	0.53				
Spindle *Z*-axis	Vibration signal	Frequency (Hz)	580.8	1012	3755	3853	3984
		Correlation coefficient	0.51	0.51	0.51	0.52	0.50
Relative vibration *Y*-axis	Vibration signal	Frequency (Hz)	3853	3984			
		Correlation coefficient	0.50	0.50			
Relative vibration *Z*-axis	Vibration signal	Frequency (Hz)	580.8				
		Correlation coefficient	0.50				

Table 9 MAPE value vs. levels of prediction performance

MAPE	Prediction performance
< 10%	Highly accurate
10%–20%	Accurate
20%–50%	Reasonable
> 50%	Not accurate

performance of the R_a prediction was assessed by the mean absolute percentage error (MAPE), that is

$$\mathrm{MAPE} = \frac{1}{n}\sum_{i=1}^{n}\left|\frac{y_i - x_i}{y_i}\right|, \tag{16}$$

where y_i represents the actual measured R_a value, x_i represents the predicted value, and n is the total number of experimental cases. The previous study of Lewis [19] indicated that the different MAPE values reveal the different levels of prediction performance which can be organized in Table 9.

Figure 6 shows the R_a prediction result of using the cutting parameters (the first class) as the input layer of back-propagation ANN (BP ANN) model. Although this figure shows that the MAPE in this experiment is 29% representing a reasonable prediction result, it still exists an amount of error that is unsatisfactory for the industrial applications. Therefore, it is intuitively inferred that the surface roughness of the workpiece is affected not only by the cutting parameters, but also by another factors, such as the oscillating phenomena induced from the tooling environment.

In the second experiment, the features of vibration signals were selected as the input layer of BP ANN model according to the Pearson correlation analysis as shown in Tables 3, 4, 5, 6, 7, and 8. The R_a prediction result of using the features of this class is shown in Fig. 7. The MAPE of 25% presents that the prediction result is reasonable. It also demonstrates that the prediction accuracy can be improved through using the vibration signal features in the time domain as well as the frequency domain.

By combining the features of the first and the second classes, the R_a prediction result of using the features of the third class as the input layer of BP ANN model is shown in Fig. 8.

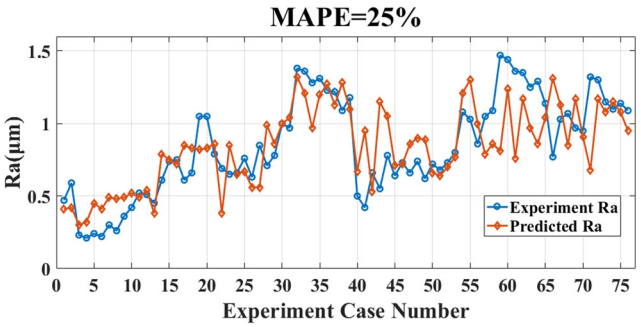

Fig. 7 R_a prediction result by using features of the second class

With the input features of the third class, the MAPE is improved to 18% representing an accurate prediction. Therefore, it is inferred that the R_a prediction performance can be enhanced by utilizing the cutting parameters and the vibration signals features. Namely, the surface roughness of the workpiece during the milling process is governed by the tooling setup conditions and the tooling environmental influence, such as the vibration manners. Therefore, an accurate prediction of workpiece surface roughness can be achieved by analyzing the information of machine vibration as well as the cutting parameters.

4 Conclusion

For the purpose of predicting the surface roughness of S45C steel in milling process, the features were extracted from the measured vibration signals and their corresponding envelopes in time domain as well as frequency domain. Through the Pearson correlation analysis, the certain features were selected according to the correlation coefficient values. The correlation analysis results show that more features on Z-axis have high correlation with the R_a values than those on the other two axes. Furthermore, the vibration signals have more highly correlated features with the R_a values than their corresponding envelope signals in the frequency domain while the corresponding envelopes have more highly correlated features with the R_a values than the vibration signals in the time domain. The results of surface roughness prediction demonstrate that the

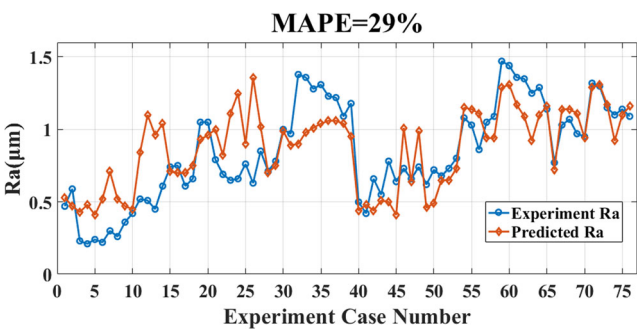

Fig. 6 R_a prediction result by using features of the first class

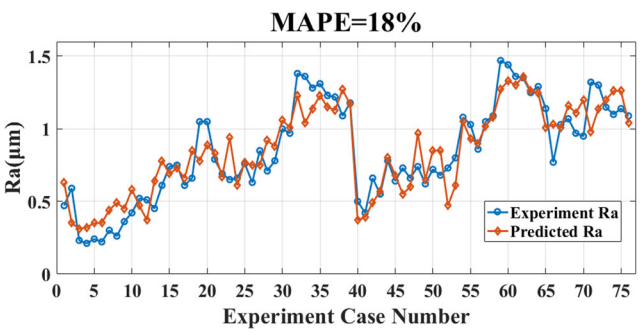

Fig. 8 R_a prediction result by using features of the third class

accuracy of R_a prediction can be enhanced through combining the selected vibration signal features and the cutting parameters as the input layer of the BP ANN model. The online measurement of cutter wear is expected to be fulfilled in the further studies so that the cutter wear can be accurately quantified instead of the estimated RVA.

Funding information This research is partially financially supported by the Ministry of Science and Technology in Taiwan, Republic of China, under the project numbers MOST 105-2221-E-005-025-MY3 and MOST 106-2218-E-194-002.

References

1. Karayel D (2009) Prediction and control of surface roughness in CNC lathe using artificial neural network. J Mater Process Technol 209:3125–3137
2. Asiltürk İ, Çunkaş M (2011) Modeling and prediction of surface roughness in turning operations using artificial neural network and multiple regression method. Expert Syst Appl 38:5826–5832
3. Chang HK, Kim JH, Kim IH, Jang DY, Han DC (2007) In-process surface roughness prediction using displacement signals from spindle motion. Int J Mach Tools Manuf 47:1021–1026
4. Abouelatta OB, Mádl J (2001) Surface roughness prediction based on cutting parameters and tool vibrations in turning operations. J Mater Process Technol 118:269–277
5. Abu-Mahfouz I, El Ariss O, Esfakur Rahman AHM, Banerjee A (2017) Surface roughness prediction as a classification problem using suport vector machine. Int J Adv Manuf Technol 92:803–815
6. Daniel KE, Chen JC (2007) Development of a fuzzy-nets-based surface roughness prediction system in turning operations. Comput Ind Eng 53:30–42
7. Yang CY, Wu TY (2015) Diagnostics of gear deterioration using EEMD approach and PCA process. Measurement 61:75–87
8. Yan R, Gao RX (2007) Approximate entropy as a diagnosis tool for machine health monitoringm. Mech Syst Signal Process 21:824–839
9. Wu TY, Yu CL, Liu DC (2016) On multi-scale entropy analysis of order-tracking measurement for bearing fault diagnosis under variable speed. Entropy 18(2):292
10. Tangjitsitcharoen S, Thesniyom P, Ratanakuakangwan S (2017) A wavelet approach to predict surface roughness in ball-end milling. Proc Inst Mech Eng B J Eng Manuf 231(14):2468–2478
11. Khorasani A, Yazdi MRS (2017) Development of a dynamic surface roughness monitoring system based on artificial neural networks (ANN) in milling operation. Int J Adv Manuf Technol 93:141–151
12. Wu TY, Lai CH, Liu DC (2016) Defect diagnostics of roller bearing using instantaneous frequency normalization under fluctuant rotating speed. J Mech Sci Technol 30(3):1037–1048
13. Huang NE, Shen Z, Long SR, Wu MC, Shih HH, Zheng Q, Yen NC, Tung CC, Liu HH (1998) The empirical mode decomposition and the Hilbert spectrum for nonlinear and non-stationary time series analysis. Proc R Soc Lond A 454:903–995
14. Shannon CE (1948) A mathematical theory of communication. Bell Syst Tech J 27:379–423
15. Richman JS, Moorman JR (2000) Physiological time-series analysis using approximate entropy and sample entropy. Am J Physiol Heart Circ Physiol 278:H2039–H2049
16. Costa M, Goldberger AL, Peng CK (2002) Multiscale entropy analysis of complex physiologic time series. Phys Rev Lett 89:068102
17. Costa M, Goldberger AL, Peng CK (2005) Multiscale entropy analysis of biological signals. Phys Rev E 71:021906
18. McClelland JL, Rumelhart DE (1986) Parallel distributed processing: explorations in the microstructure of cognition 1. MIT Press
19. Lewis CD (1982) Industrial and business forecasting methods. Butterworths, London